Environmental Science and Pollution Research (2023) 30:75247–75261
https://doi.org/10.1007/s11356-023-27674-y

RESEARCH ARTICLE

# Construction of $Co_3O_4$ anchored on $Bi_2MoO_6$ microspheres for highly efficient photocatalytic peroxymonosulfate activation towards degradation of norfloxacin

**Qing Sun[1] · Xiaofang Hu[1] · Yingjie Zhao[1] · Jian Zhang[1] · Jiawei Sheng[1]**

Received: 1 February 2023 / Accepted: 11 May 2023 / Published online: 22 May 2023


## Abstract

Dissolved antibiotics have been a research subject due to their widespread presence and potential threats in drinking water treatment. To enhance the photocatalytic activity of $Bi_2MoO_6$ for the degradation of norfloxacin (NOR), the heterostructured $Co_3O_4/Bi_2MoO_6$ (CoBM) composites were synthesized by employing ZIF-67-derived $Co_3O_4$ on $Bi_2MoO_6$ microspheres. The as-synthesized resultant material 3-CoBM by 300 °C calcination was characterized by XRD, SEM, XPS, transient photocurrent techniques, and EIS. The photocatalytic performance was evaluated by monitoring different concentrations, NOR removal from aqueous solution. Compared with $Bi_2MoO_6$, 3-CoBM exhibited the better adsorption and elimination capacity of NOR due to the combined effect between peroxymonosulfate activation and photocatalytic reaction. The influences of catalyst dosage, PMS dosage, various interfering ions ($Cl^-$, $NO_3^-$, $HCO_3^-$, and $SO_4^{2-}$), pH value, and type of antibiotics for application removal were also invested. By activating PMS under visible-light irradiation, 84.95% of metronidazole (MNZ) can be degraded within 40 min, and NOR and tetracycline (TC) can be completely degraded using 3-CoBM. Degradation mechanism was elucidated by quenching tests in combination with EPR measurement, and the degree of activity of the active groups from strong to weak is $h^+$, $SO_4^{-}\bullet$, and •OH, respectively. The degradation products and conceivable degradation pathways of NOR were speculated by LC-MS. In combination of excellent peroxymonosulfate activation and highly enhanced photocatalytic performance, this newly $Co_3O_4/Bi_2MoO_6$ catalyst might be a promising candidate for degrading emerging antibiotic contamination in wastewater.

**Keywords** $Co_3O_4$ · $Bi_2MoO_6$ · Peroxymonosulfate · Photocatalytic degradation · Norfloxacin

## Abbreviations

| | |
|---|---|
| CoBM | $Co_3O_4/Bi_2MoO_6$ |
| NOR | norfloxacin |
| MNZ | metronidazole |
| TC | tetracycline |
| AOPs | advanced oxidation processes |
| *k* | rate constant of reaction |
| 2D | two-dimensional |
| PMS | peroxymonosulfate |
| PDS | peroxydisulfate |
| 2-MIN | 2-methylimidazole |
| TBA | tert-butanol |
| SEM | scanning electron microscopy |
| XRD | X-ray diffraction |
| TEM | transmission electron microscope |
| XPS | X-ray photoelectron spectroscopy |
| EIS | electrochemical impedance spectra |
| EPR | electron paramagnetic resonance |
| LC-MS | liquid chromatography-mass spectrometry |
| ROS | reactive oxygen species |

Responsible Editor: Sami Rtimi

✉ Jiawei Sheng
jw-sheng@zjut.edu.cn

[1] College of Materials Science and Engineering, Zhejiang University of Technology, Hangzhou 310014, China

## Introduction

Norfloxacin (NOR), as one of the third generation of quinolone antibacterial drugs, has been widely applied in the treatment of respiratory, pneumonia, urinary tract infections, bronchitis, enteritis, gonorrhea, and other bacterial infections (González-Pleiter et al. 2013, Wang et al. 2019b). Due to its widespread use, chemical stability, persistence, moderate aqueous solubility, and poor biodegradability, NOR has

always been a ubiquitous contaminant in water bodies, which may cause severe damage to aquatic ecosystems and potential noxious effects on human beings (Wammer et al. 2013). Consequently, it is of great significance to develop effectively technologies for NOR removal from polluted water. Traditionally, adsorption is the most conventional treatment processes for NOR removal. But adsorption involves low adsorption capacity, and the generation of secondary toxic products cause further damage to the environment (Biswal & Balasubramanian 2022). Therefore, it is desirable to establish a well-developed and effective water treatment method for NOR removal.

Up to now, numerous techniques were developed to eliminate noxious NOR contaminant from wastewater that comprised biological oxidation, membrane filtration, flocculation, coagulation, chemical oxidant-induced advanced oxidation processes (AOPs) such as $O_3$ oxidation, Fenton, photocatalysis, electrochemical oxidation, electrochemical-Fenton (EF), and combined processes (Alizadeh et al. 2023, García-Muñoz et al. 2019, Özcan et al. 2016, Pan et al. 2022). From an energy perspective, most of these wastewater treatment methods are neither economical nor effective. Among them, photocatalysis is comparatively considered as a potential approach for its significant advantages of low energy consumption, green environmental protection, and absolute degradation or mineralization of the refractory contaminants such as NOR (Cai et al. 2023, Wang et al. 2021b). To achieving a high-rate constant ($k$) for photocatalytic degradation with under visible light irradiation, bismuth-based photocatalysts such as $Bi_2O_3$, $BiVO_4$, $Bi_2MoO_6$, BiOBr, BiOCl, $Bi_2Sn_2O_7$, and $BiFeO_3$ have attracted great attention in photocatalytic removal of hazardous contaminants from water due to their outstanding properties including low toxicity, stability, and economy (Senasu et al. 2021, Sun et al. 2022c, Wu et al. 2022, Yin et al. 2022). Especially, $Bi_2MoO_6$ is a two-dimensional (2D) compound composed of positively charged layers and interlayer anions, which is considered to be an alternative material with poor visible light capture ability such as $TiO_2$, ZnO, and $SnO_2$ (Sun et al. 2021).

However, the photocatalytic degradation technology based on the single $Bi_2MoO_6$ is far from practical application due to its high $e^-$-$h^+$ recombination rate, low quantum efficiency, and poor adsorption (Wang et al. 2020a). The half-life of hydroxyl radical (•OH), the most active radical generated in the process of photocatalysis, is too short to guarantee oxidation degradation of organic pollutants, which will also lead to the reduction of photocatalytic efficiency. The use of sulfate ($SO_4^-$•) radical-based processes have also become more attractive owing to the advantages of such radicals over •OH (Alizadeh & Rezaee 2022). Furthermore, NOR is a thermodynamically stable and kinetically inert molecule that requires high electrical energy to attack sites with high electron density on the phenyl and piperazine rings (Zhu et al. 2023). To solve these problems, the sulfate radical ($SO_4^-$•) based on persulfate advanced oxidation technology (SR-AOPs) has been widely concerned. Compared with photocatalysis, persulfate activation has strong standard redox potentials ($E_0(SO_4^-•/SO_4^{2-})$ = 2.6–3.1 $V_{NHE}$ vs. $E_0$(•OH/$OH^-$) = 1.9−2.7 $V_{NHE}$), a longer half-life (30−40 μs), less dependence on pH, non-toxicity, and easy transportation, resulting in higher NOR degradation efficiency (Aseman-Bashiz et al. 2021, Wang et al. 2019a, Wang et al. 2022, Wu & Kim 2022). Up till now, many studies have shown that the $SO_4^-$• can be generated from peroxymonosulfate (PMS) or persulfate (PS) by the activation of various transition metals (such as Co, Ni, Mn, Cu, Fe, and Ru) (Alhamd et al. 2021, Ghanbari & Moradi 2017, Peng et al. 2021, Wang et al. 2020b). Compared with other transition metals, cobalt-based catalysts are considered to be the most effective PMS activator through a rapid reversible redox process. However, pure cobalt-based catalysts are inevitably accompanied by the toxicity of Co ions leaching, which may cause secondary pollution in the solution (Gao et al. 2019).

More recently, Zhang et al. (2021) found that adding PMS as an electron acceptor to the photocatalytic system could not only improve the separation of $e^-$-$h^+$ but also increase the production of $SO_4^-$• free radical, achieving a synergistic effect. Feng et al.'s (2019) work also confirmed that prepared $Bi_2MoO_6$ nanosheets can degrade tetracycline hydrochloride with an efficiency of 83% under the combination of visible light and PS, which was much higher than that of Vis/$Bi_2MoO_6$ system (about 48.2%). Guo et al. (2021) recently synthesized $Bi_2MoO_6$ nanoplates with PVP as an active agent and combined $Co_3O_4$ by precipitation process to obtain $Co_3O_4$@$Bi_2MoO_6$, which can activate PMS for degrading 87.68% of norfloxacin within 30 min under visible light illumination. In order to further reduce the harm of cobalt and improve the activation ability, a new type of low Co-containing substance with the synergistic catalytic activation of the SR-AOPs will be an effective strategy for the green, efficient, and sustainable degradation of organic pollutants under moderate conditions. Consequently, it is highly valuable to develop cobalt-bismuth composite photocatalyst that promote SR-AOPs process while improving NOR degradation.

At present, the size of nano-catalysts containing cobalt-bismuth heterostructure is usually uneven with irregular morphology. Nevertheless, it has been proved that the photocatalysts were significantly affected by factors such as preparation method and morphology. Catalytic degradation reactions usually occur first on the surface and then from outside to inside, while the spherical shape usually has the largest specific surface area and favors full exposure of response sites. And if the harmful metal cobalt loads on the spherical surface, it is more conducive to reduce its use and give fully exerting activation effect of the PMS. Therefore,

how to further improve the dispersion and effective utilization of cobalt metals by adjusting the morphology and structure and thereby enhance the photocatalysis-activated PMS performance of cobalt-bismuth photocatalysts still needs in-depth research.

Thus, based on the above considerations, this manuscript reports innovative research based on heterostructured $Co_3O_4$/$Bi_2MoO_6$ (CoBM) composites synthesized by employing ZIF-67-derived $Co_3O_4$ anchored on $Bi_2MoO_6$ microspheres with the significantly synergy of photocatalytic and peroxymonosulfate activity. Owing to its high separation rate of photogenerated $e^-$-$h^+$ pairs and peroxymonosulfate activity, 3-CoBM by 300 °C calcination can effectively remove 100% of NOR within 40 min. In combination of quenching tests and EPR, the radical quenching measurement proved that the photoproduction hole ($h^+$), sulfate ($SO_4^-$•), and hydroxyl (•OH) had been indicated as the primary radicals. The possible degradation mechanism and pathway of NOR were also proposed. This novel 3-CoBM catalyst may be a promising candidate for degradation of the main sources of antibiotic contamination sources in pharmaceutical wastewater.

## Experiment

### Materials

$Bi(NO_3)_3{\cdot}5H_2O$, 2-methylimidazole (2-MIM) and tetracycline ($C_{22}H_{24}N_2O_8$) were obtained from Maclean Biochemical Technology Co., Ltd. $(NH_4)_6Mo_7O_{24}{\cdot}4H_2O$, $NaHCO_3$, $C_2H_5OH$, ethylene glycol ($C_2H_6O_2$), $CH_3OH$, and NaOH were purchased form Sinopharm Chemical Reagent Co., Ltd. $Co(NO_3)_2{\cdot}6H_2O$, norfloxacin ($C_{16}H_{18}FN_3O_3$), and metronidazole ($C_6H_9N_3O_3$) were purchased from the Aladdin Biochemical Technology Co., Ltd. HCl were purchased from Yongle Chemical Technology Co., Ltd. (Jiangsu, China). All chemicals were analytical grade reagents and were used as received without further purification. The distilled (DI) water was used throughout this work.

### Preparation of samples

(a) Preparation of $Bi_2MoO_6$

1.94 g $Bi(NO_3)_3{\cdot}5H_2O$ was added to 25 mL of ethylene glycol (EG) and sonicated for 10 min to obtain solution A. At the same time, 0.35 g of $(NH_4)_6Mo_7O_{24}{\cdot}4H_2O$ was added to 5 mL of deionized water for uniform dispersion, followed by 15 mL of ethanol (EtOH), and ultrasonicated for 10 min to obtain solution B. Subsequently, solutions A and B were mixed and stirred for another 0.5 h until they were completely fused. Finally, the mixed solution was transferred to an autoclave for reaction at 160 °C for 14 h, washed with deionized water and ethanol, which was dried at 60 °C for 8 h, and treated at 400 °C for 1 h to obtain bright yellow $Bi_2MoO_6$ microsphere.

(b) Synthesis of $Co_3O_4$

0.291 g $Co(NO_3)_2{\cdot}6H_2O$ was added to 15 mL of MeOH obtained solution a. Meanwhile, 0.328 g 2-methylimidazole was dispersed in 15 mL of MeOH, poured into a, stirred for 30 min, and aged for 24 h. Subsequently, the aged solution was filtered and separated to obtain powder, which was washed three times with ethanol and deionized water and dried in a vacuum drying oven at 60 °C for 8 h. Finally, the dried powder was subjected to the final calcination treatment. The powder was placed in a tube furnace in an air atmosphere and treated at 300 °C (400 °C, 500 °C) for 2 h at the heating rate of 2 °C/min to obtain $Co_3O_4$. The $Co_3O_4$ was denoted as $x$-$Co_3O_4$ ($x$ means to the calcination temperature).

In addition, the preparation of ZIF-67 is the same as above, without the last step of calcination, and the bright purple powder after separation and drying is ZIF-67.

(c) Synthesis of $Co_3O_4$/$Bi_2MoO_6$

0.895 g $Bi_2MoO_6$ was dispersed in 15 mL methanol (MeOH), and 0.291 g $Co(NO_3)_2{\cdot}6H_2O$ was added to form solution C. Meanwhile, 0.328 g of 2-methylimidazole (2-MIN) was dispersed in 15 mL of MeOH, poured into solution C, stirred for 30 min, and aged for 24 h. Subsequently, the aged solution was filtered and separated to obtain powder, which was washed three times with ethanol and deionized water and dried in a vacuum drying oven at 60 °C for 8 h. Finally, the dried powder was subjected to the final calcination treatment. The powder was placed in a tube furnace in an air atmosphere, treated at 300 °C (400 °C, 500 °C) for 2 h at the heating rate of 2 °C/min to obtain $Co_3O_4$/$Bi_2MoO_6$ hybrid catalyst. The $Co_3O_4$/$Bi_2MoO_6$ denoted as $y$-CoBM ($y$ means to the calcination temperature) (Scheme 1).

### Catalyst characterizations

The crystal structures of the synthesized samples were analyzed by X-ray diffraction (XRD) analyzer. The patterns were measured in the $2\theta$ range of 5–80° with Ultima IV X-ray diffractometer (Rigaku, Cu Kα, $\lambda = 0.15406$ nm). The microstructure and size distribution of the sample were observed by Tecnai G2 F30 transmission electron microscope (TEM). The microstructure was analyzed by nanonova 450 field emission scanning electron microscope (SEM). The elemental composition on the surface of the material and the corresponding chemical valence state of the element were obtained by X-ray photoelectron spectroscopy (XPS, Thermo Scientific K-Alpha).

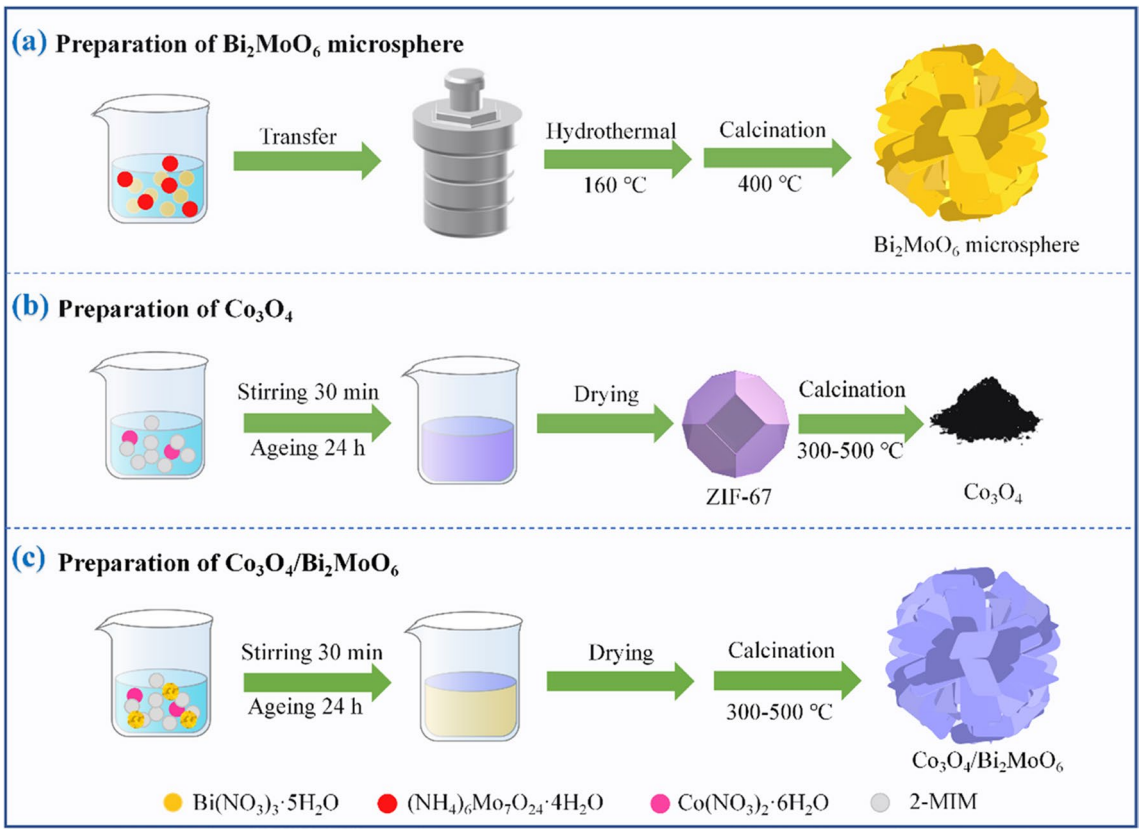


**Scheme 1** Preparation of $Bi_2MoO_6$, $Co_3O_4$, and $Co_3O_4/Bi_2MoO_6$ samples

### Degradation testing

A 300-W halogen tungsten lamp with a 420 nm filter was used to simulate visible light to simulate the photocatalytic degradation of antibiotics in wastewater. Norfloxacin (NOR), tetracycline (TC), and metronidazole (MNZ) were used as target degradation products. The photocatalytic performance of the prepared catalysts was tested by detecting the degradation efficiency of the target degradants. Absorbance was measured with a spectrophotometer (UV-2550). The free radicals were identified adopted to electron paramagnetic resonance (EPR, Bruker A300-10/12). The degradation intermediates of NOR were detected by liquid chromatography-mass spectrometry (LCMS) operating an Agilent 1100 HPLC system coupled to a Thermos TSQ Quantum Ultra mass spectrometer.

## Results and discussion

### Characterization of composites

#### XRD

XRD analysis was subjected for all the synthesized samples in Fig. 1. The crystallinity and purity of the prepared single-component $Bi_2MoO_6$, the $Co_3O_4$ derived from ZIF67 at 300 °C, and the composite of both obtained at 300 °C (3-CoBM) are shown in Fig. 1a, b. The diffraction angles at 10.9°, 23.5°, 28.2°, 32.5°, 36.1°, 47.1°, 55.5°, and 58.5° were compared to the (020), (111), (131), (200), (151), (260), (133), and (262) crystal planes of $Bi_2MoO_6$ (JCPDS No. 21-0102), respectively. Besides, the diffraction peaks have sharp peak shapes, which indicates the synthesis of $Bi_2MoO_6$ with good crystallinity. The peak at 36.9° is compared to the crystal plane of (311) of $Co_3O_4$ (JCPDS No. 42-1467), which can be observed in the XRD spectrum of the corresponding $Co_3O_4$. In addition, the identifiable diffraction peaks in XRD spectra of 3-CoBM composites correspond well to the pure $Bi_2MoO_6$, and there are no offset and no other impurities. At the same time, no obvious diffraction characteristic peaks of $Co_3O_4$ appear, which may be caused by the low content of $Co_3O_4$ in 3-CoBM. This is not the first time that such phenomena have been observed in studies (Gao et al. 2018, Tang et al. 2016). It is worth noting that the XRD spectrum of 3-CoBM did not show any heterogeneous peaks, and the introduction of $Co_3O_4$ did not change the crystalline phase of $Bi_2MoO_6$, which indicates the high purity of the synthesized 3-CoBM series composites.

Figure 1c shows the XRD patterns of $Co_3O_4/Bi_2MoO_6$ composites obtained at different calcination temperatures.

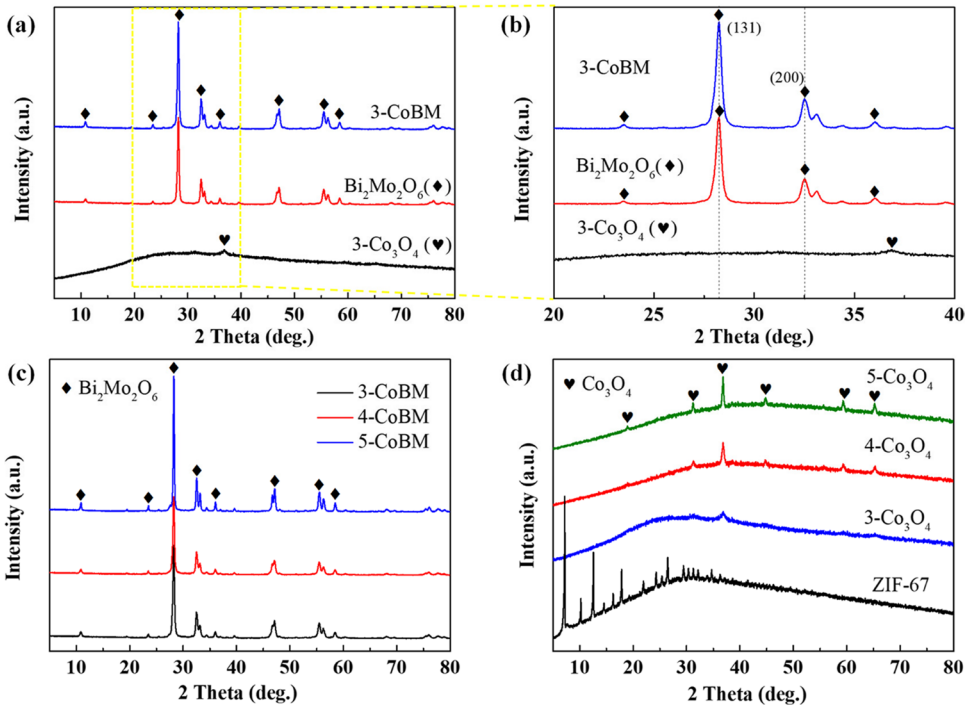


**Fig. 1** XRD patterns of samples. **a** 3-$Co_3O_4$, $Bi_2MoO_6$, and 3CoBM; **b** enlarged patterns between 20 and 40°; **c** $Co_3O_4$/$Bi_2MoO_6$ composites obtained at different calcination temperatures; **d** $Co_3O_4$ obtained at different calcination temperatures of ZIF-67 and ZIF-67

The $Co_3O_4$/$Bi_2MoO_6$ material's peak shape and position did not dramatically change over time; the peak did become sharper as the temperature increased. However, no obvious $Co_3O_4$ diffraction peaks were observed even when the temperature was increased to 500 °C. Figure 1d illustrates the effect of temperature on the transformation of ZIF-67 to $Co_3O_4$. To demonstrate the synthesis of ZIF-67, one of the spectral lines corresponding to it can be compared to the XRD spectrum in the literature (Sun et al. 2022a, Zhou et al. 2017). As the temperature rises, the distinctive diffraction peaks of $Co_3O_4$ get stronger and stronger.

## SEM

The morphologies of ZIF-67, 5-$Co_3O_4$, $Bi_2MoO_6$, and 3-CoBM composites were characterized by SEM, and the results are illustrated in Fig. 2. As displayed in Fig. 2a, the rhombic dodecahedron morphology of the synthesized ZIF-67 has a particle size of roughly 600 nm, and the overall morphology is irregular with local aggregation. As depicted in Fig. 2b, ZIF-67 transformed from a vivid purple powder to a fluffy black powder ($Co_3O_4$) after being held at 500 °C for 2 h, and the SEM image showed irregular aggregated adhesion. Figure 2c, d further demonstrates that $Bi_2MoO_6$ is composed of nano-microspheres with diameters of 1~3 μm, which are formed by stacks of short nanorods. In contrast to pure $Bi_2MoO_6$, Fig. 2e, f indicates that the morphology of nanorods on the surface of 3-CoBM microspheres is mostly hidden, demonstrating that a layer of $Co_3O_4$ has been successfully compounded on top of $Bi_2MoO_6$ microspheres. The morphology of 3-CoBM is also 1~3-nm nanospheres. The powder color also changed from the bright yellow of pure $Bi_2MoO_6$ to brownish brown.

## XPS

As displayed in Fig. 3, the chemical composition and state of the prepared 3-CoBM were verified by XPS. Figure 3a shows that 3-CoBM contains four elements: Bi, Mo, O, and Co, with C being an exotic C introduced during the testing process. The high-resolution XPS spectra of Bi 4f, Mo 3d, O 1s, and Co 2p of the 3-CoBM material are shown in Fig. 3b–e, while these XPS spectra are corrected for the C1s peak (284.8 eV). In Fig. 3b, the two peaks at binding energies 159.26 eV and 164.56 eV are assigned to Bi $4f_{7/2}$ and Bi $4f_{5/2}$ orbits, indicating that Bi element exists in $Bi^{3+}$ state in the 3-CoBM material (Chen et al., 2019, Shen et al. 2020a). As presented in Fig. 3c, the binding energies located at 232.53 eV and 235.67 eV in the Mo 3d peak correspond to Mo $3d_{5/2}$ and Mo $3d_{3/2}$ of $Mo^{6+}$ (Zhao et al. 2016), which can demonstrate the presence of positive hexavalent Mo ions in 3-CoBM. In addition, as shown in Fig. 3d, the binding energies of 530.15 eV and 531.70 eV correspond to lattice oxygen on the surface of $Bi_2MoO_6$ and oxygen in adsorbed water, respectively (Shen et al. 2020b), where the lattice oxygen binding energy position of $Co_3O_4$ is at 530 ± 0.2 eV (Lu et al. 2014), which is quite close to the position of lattice oxygen on the surface of $Bi_2MoO_6$. The Co 2p peak of 3-CoBM is depicted in Fig. 3e, where $Co^{3+}$ corresponds to peaks with binding energies of 780.00 eV and 795.30 eV,

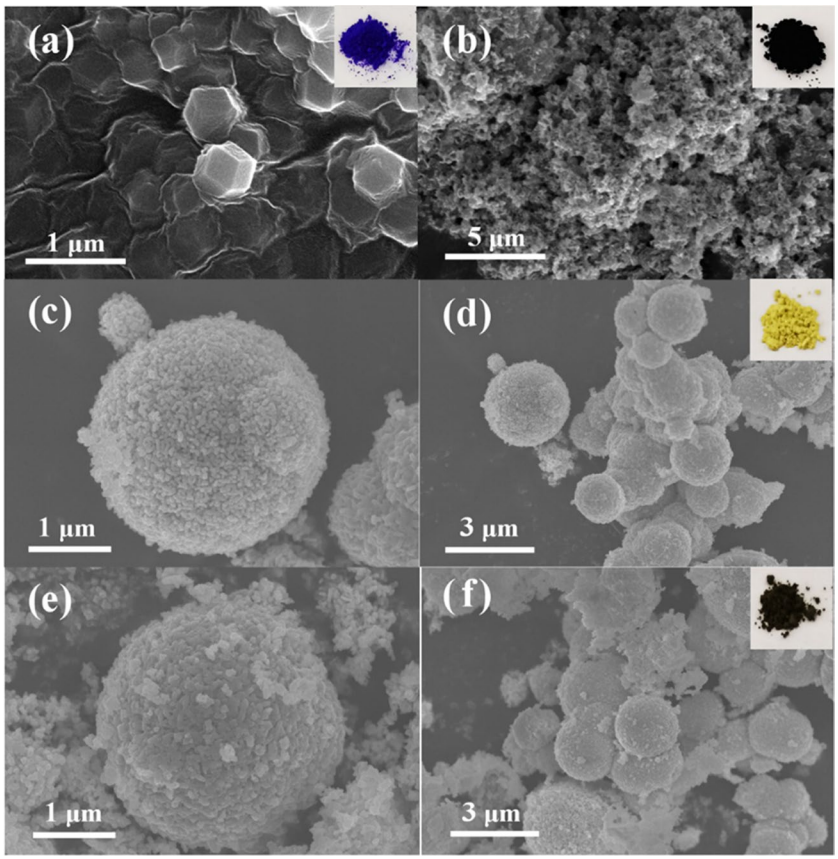


**Fig. 2** **a** SEM image of ZIF67; **b** SEM image of 5-$Co_3O_4$; **c**, **d** SEM images of $Bi_2MoO_6$ at different magnifications; **e**, **f** SEM images of 3-CoBM at different magnifications

while $Co^{2+}$ is located at peaks of 781.80 eV and 796.70 eV, respectively (Li et al. 2020, Shen et al. 2020a). The formation of $Co_3O_4$ was further confirmed by XPS, indicating that $Co_3O_4$/$Bi_2MoO_6$ composite catalytic materials with strong interactions have been obtained

### Photocurrent response and EIS

To evaluate the interfacial charge transfer and separation efficiency of $Bi_2MoO_6$ and 3-CoBM materials, photocurrent and electrochemical impedance tests were performed, and the results are illustrated in Fig. 4. Figure 4a shows that the photocurrent response of 3-CoBM is much higher that of single-component $Bi_2MoO_6$ under the same conditions, indicating that the heterojunction formed by $Co_3O_4$ and $Bi_2MoO_6$ contributes to the generation and transfer of photogenerated carriers. The Nyquist curve appears semicircular; a smaller arc radius of the impedance spectrum implies better separation of the electron-hole and a faster photocatalytic reaction rate (Wen et al. 2018a). The EIS data in Fig. 4b suggests that 3-CoBM has a smaller arc radius compared to $Bi_2MoO_6$, and it can be concluded that the $Co_3O_4$/$Bi_2MoO_6$ hetero-junction can simultaneously speed up electron transport and enhance the separation efficiency of photogenerated electron-hole pairs.

## Degradation performance

### Comparison of catalytic activity of catalysts in different systems

To investigate the adsorption performance of $Co_3O_4$, $Bi_2MoO_6$, and $Co_3O_4$/$Bi_2MoO_6$ (3-CoBM) on NOR, the adsorption capacity of the three samples was observed under an environment with complete darkness for half an hour. The results are shown in Fig. 5; the most effective adsorption material was $Co_3O_4$, followed by 3-CoBM, while $Bi_2MoO_6$ was the least effective adsorption material. The excellent adsorption capacity of $Co_3O_4$ originates from the retention of the porous structure of the MOFs material, so the adsorption capacity of the 3-CoBM composites is somewhat improved compared with $Bi_2MoO_6$. Meanwhile, the desorption equilibrium was reached within 30 min for all three materials, to make the best use of time, the dark treatment time for all subsequent experiments in 30 min.

So, as to evaluate the effect of different calcination temperatures on the catalytic activity of $Co_3O_4$/$Bi_2MoO_6$ series composites, three temperature ranges of 300 °C, 400 °C, and 500 °C were investigated. The degradation efficiency of NOR under the conditions of visible light irradiation

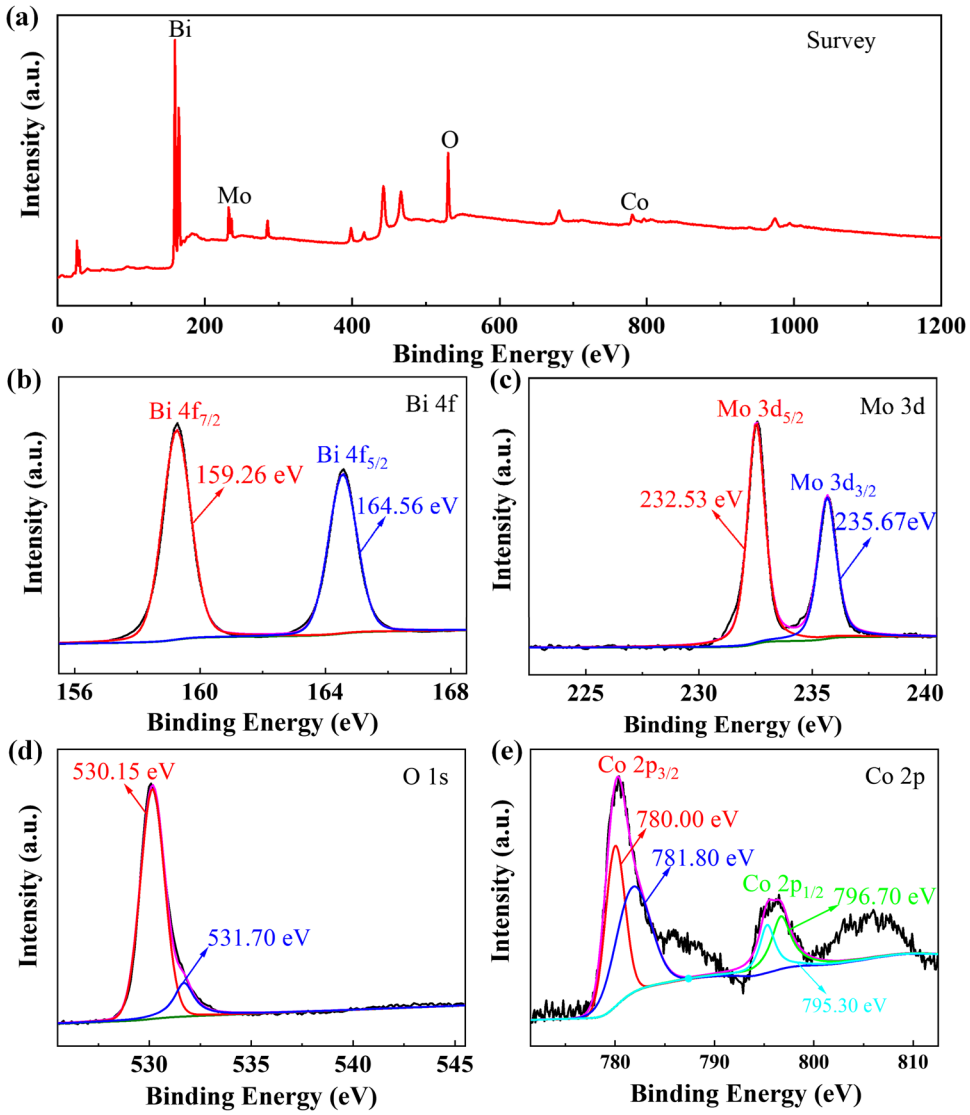


**Fig. 3** XPS spectra of 3-CoBM sample. **a** Survey, **b** Bi 4f, **c** Mo 4d, **d** O 1s, and **e** Co 2p

and PMS and the result are demonstrated in the Fig. 6. Clearly, the degradation capacity of pure $Bi_2MoO_6$ is non-ideal; the degradation rate of NOR by single-component $Bi_2MoO_6$ was only 23.75% in 40 min as shown in Fig. 6a. The 3-CoBM composites calcined at 300 °C showed the highest catalytic activity for NOR, and the degradation rate of NOR achieved 100% within 40 min. The catalytic activity of 4-CoBM decreases significantly with increasing

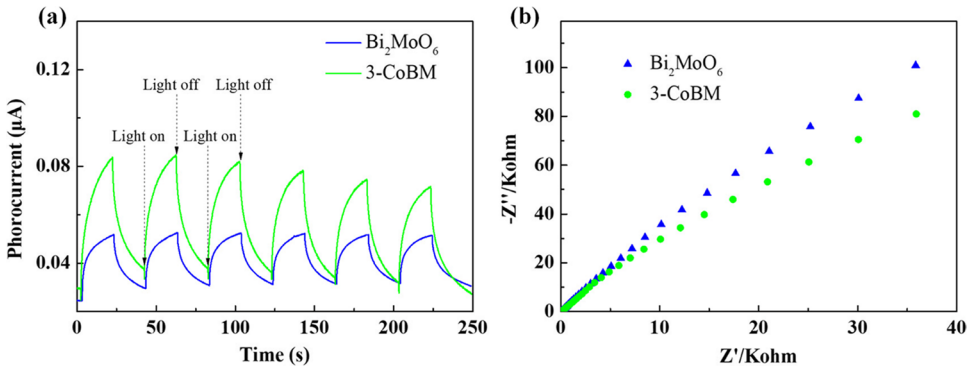


**Fig. 4** **a** Photocurrent response spectra and **b** electrochemical impedance spectra (EIS) of $Bi_2MoO_6$ and 3-CoBM samples

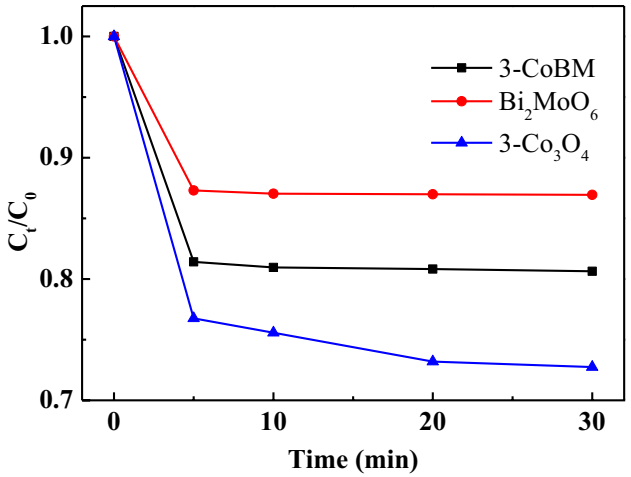


**Fig. 5** Absorption ability evaluation of the $Co_3O_4$, $Bi_2MoO_6$, and 3-CoBM for NOR in dark condition (NOR = 20 mg/L, 3-$Co_3O_4$, $Bi_2MoO_6$ or 3-CoBM = 30 mg)

calcination temperature; the degradation efficiency of NOR in 40 min was 79.58%. At the same time, the degradation rate decreases rapidly as calcination temperature increases from 400 to 500 °C, and the degradation efficiency of NOR was 68.76% for 5-CoBM in just 40 min.

To assess the impact of temperature and the function of $Co_3O_4$ even more, the pseudo-first-order kinetics was employed to calculate the degradation rate of the NOR removal process as shown in Fig. 6b. The fitted reaction constant ($k_{obs}$) value of 3-CoBM-vis-PMS is approximately 28 times higher than that of $Bi_2MoO_6$-vis-PMS, manifesting that the $Co_3O_4$ has a key point effect on vis-PMS. The $k_{obs}$ of the 3-CoBM-vis-PMS was about 4.1 times and 5.8 times that of 4-CoBM-vis-PMS and 5-CoBM-vis-PMS. It can be clearly observed that the catalytic activity of the composite catalyst decreases significantly with the increase of temperature. The reason for this phenomenon can be reasonably inferred that $Bi_2MoO_6$ catalytic activity decreases and the structure of ZIF-67 are gradually destroyed with increasing temperature (Jadhav et al. 2022, Li et al. 2022).

$$-\ln\left(C_t/C_0\right) = k_{obs}t \quad (1)$$

To study the catalytic activity of 3-CoBM in different systems, several systems were constructed as shown in Fig. 6c. It can be observed that 3-CoBM-vis-PMS exhibited the strongest catalytic activity and could completely degrade NOR within 40 min, followed by the 3-CoBM-PMS system, whereas the catalytic activity of the 3-CoBM-vis system is not as good as that of the vis-PMS system, demonstrating the significance of PMS in the system. The apparent rate constants of NOR degradation were obtained by fitting a first-order equation along Eq. (1), and the results are shown in Fig. 6d to further assess the catalytic activity of 3-CoBM. As displayed in Fig. 6d, the $k_{obs}$ of the 3-CoBM-vis-PMS system was 4.4 times higher than that of the 3-CoBM-PMS system, demonstrating that visible light is essential to the 3-CoBM-vis-PMS deterioration system. Furthermore, the $k_{obs}$ of the 3-CoBM-vis-PMS system was 25.7 times higher than that of vis-PMS, indicating that the activation of 3-CoBM is obvious and that PMS requires the activation of 3-CoBM to produce active groups and thus to be effective. The findings of the study and comparison of the three different catalytic materials 3-$Co_3O_4$, $Bi_2MoO_6$, and 3-CoBM are displayed in Fig. 6e, f. Figure 6e, f shows that the catalytic activity of 3-CoBM is superior to that of 3-$Co_3O_4$ and then superior to that of $Bi_2MoO_6$.

### Effect of reaction conditions on the degradation

Figure 7a shows the NOR degradation performance of the 3-CoBM-vis-PMS with various PMS dosages. The NOR degradation efficiency improves significantly with the increase NOR PMS dosage because the higher PMS density can augment the generation of radicals. With a PMS dosage of 25 mg, NOR can be completely degraded in 40 min. By raising the PMS concentration to 30 mg, the degradation efficiency increased slightly, indicating that the suitable dosage of PMS in the system was 25 mg. Experiments were conducted to test the 3-CoBM-vis-PMS system's response to antibiotic concentration, and if the system can successfully breakdown a variety of antibiotics, the results are given in Fig. 7b. As shown in Fig. 7b, 20 mg/L is the most suitable degradation concentration that in the degradation of NOR. The degradation efficiency could be affected with too high or too low concentration. And more notably, the degradation efficiency of low concentration (10–20 mg/L) was higher than that of high concentration, and the degradation rate was above 64% within 40 min. The effect of catalyst dosage on NOR degradation in the 3-CoBM-vis-PMS system as shown in Fig. 7c. The system's capacity to degrade to NOR steadily improves with an increase in catalyst dosage. However, when the catalyst dosage was greater than 30 mg, the degradation rate decreased rather than increased, which could indicate that the catalyst dosage was not a key factor affecting the catalytic activity of the 3-CoBM-vis-PMS system.

Activation of PMS is affected by multiple parameters; the pH value of PMS system is a key element affecting on the production reactive oxygen species. Figure 7d is the influence of pH range of 3.0 to 11.0 on the degradation of NOR by 3-CoBM-vis-PMS system. As displayed in Fig. 7d, the degradation rate of 3-CoBM-vis-PMS system reached 100% at pH = 7, and it has the best photocatalytic performance for NOR in this pH value environment. Furthermore, the degradation efficiencies of NOR were 56.71%, 66.89%, 72.82%, and 26.51% at pH = 3, 5, 9, and 11, respectively. It can be clearly observed that the degradation efficiency of

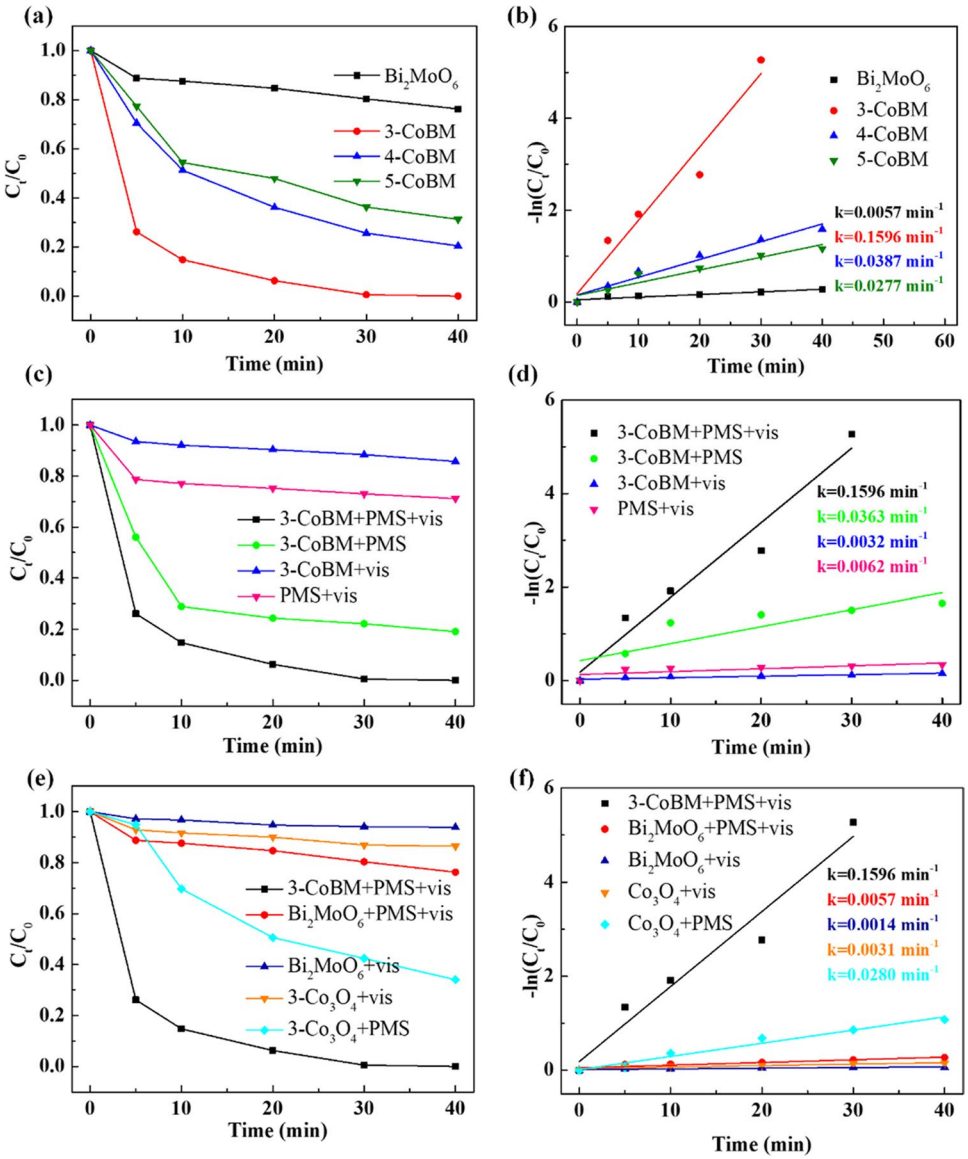


**Fig. 6** **a** Degradation curves of $Bi_2MoO_6$ and $Co_3O_4/Bi_2MoO_6$ catalysts obtained at different calcination temperatures for NOR; **b** kinetic fitting curve corresponding to degradation curve (NOR = 20 mg/L, PMS = 25 mg, $Bi_2MoO_6$ or CoBM = 30 mg); **c** NOR degradation curves of 3-CoBM in different vis-PMS systems; **d** corresponding kinetic fitting curves in different vis-PMS systems; **e** NOR degradation curves of 3-$Co_3O_4$, $Bi_2MoO_6$, and 3-CoBM in different systems; **f** corresponding kinetic fitting curves in different systems (NOR = 20 mg/L, PMS = 25 mg, 3-$Co_3O_4$, $Bi_2MoO_6$, or 3-CoBM = 30 mg)

3-CoBM-vis-PMS system to NOR becomes poor when the pH value is less than 5. The main reason for the deterioration is that the production of •OH and $SO_4^-$• will be hindered by $H^+$, the number of active free radicals is also relatively reduced to a certain extent (Huang et al. 2020).

The degradation efficiency of the system decreases under alkaline conditions (pH = 9); Eq. (2) explains it by pointing out that because of the fast kinetic reaction involved, the •OH and $SO_4^-$• generated in this environment will be quickly consumed (Sayed et al. 2017), lowering the pace at which NOR degrades.

$$SO_4^- \bullet + \bullet OH \rightarrow HSO_5^- \quad k = 1.0 \times 10^{10}\ M^{-1}s^{-1} \tag{2}$$

$$SO_4^- \bullet + \bullet OH \rightarrow SO_4^- + \bullet OH \quad k = 6.5 \times 10^{7}\ M^{-1}s^{-1} \tag{3}$$

The breakdown of NOR in a strongly alkaline environment considerably worsened with an increase in pH (pH = 11). Equation (3) provides an explanation for this phenomenon: as alkalinity rises, more $SO_4^-$• is consumed, resulting in a further decline in the quantity of free radicals that are actively reacting (Hassani et al. 2020). Additionally, PMS will deprotonate to the less oxidizing $SO_5^{2-}$ in alkaline circumstances (Guo et al. 2021). At the same time, with the increase of pH, the •OH also decreases accordingly (Ghanbari & Martínez-Huitle 2019). The results shown that real water bodies can be treated using the 3-CoBM-vis-PMS method within a specific pH range.

To demonstrate the environmental adaptability of $Co_3O_4/Bi_2MoO_6$ series composites, the effect of different interfering ions on the degradation efficiency of the system is investigated

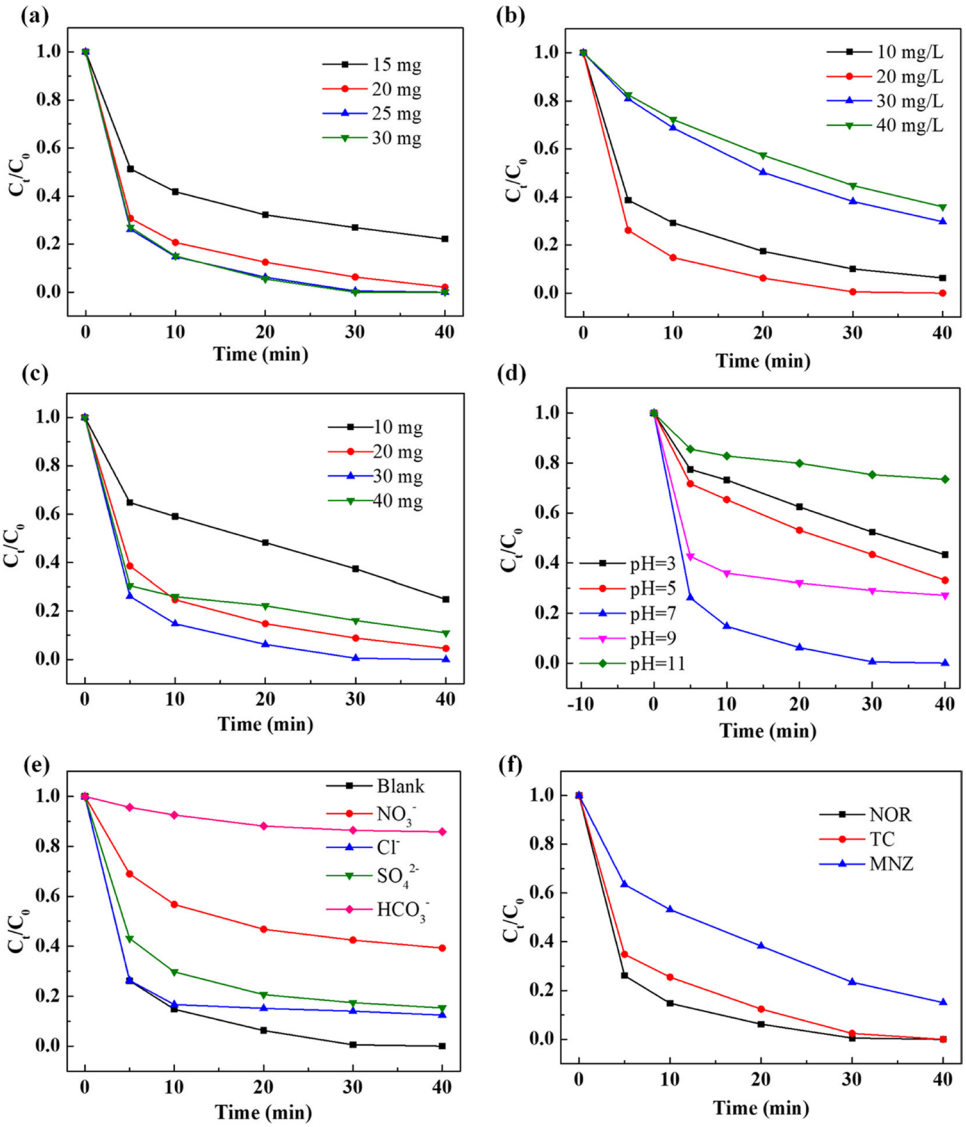


**Fig. 7** **a** Degradation curves of NOR under different amounts of PMS (NOR = 20 mg/L, PMS = 15~30 mg, 3-CoBM = 30 mg); **b** degradation curves of NOR at different concentrations in 3-CoBM-vis-PMS system (NOR = 10~40 mg/L, PMS = 25 mg, 3-CoBM = 30 mg); **c** effect of different catalyst dosage on NOR degradation (NOR = 20 mg/L, PMS = 25 mg, 3-CoBM = 10~40 mg); **d** effect of different pH on degradation of NOR (NOR = 20 mg/L, PMS = 25 mg, 3-CoBM = 30 mg); **e** effects of common anions on the degradation of NOR (200 mM, NOR = 20 mg/L, PMS = 25 mg, 3-CoBM = 30 mg); **f** degradation curves of NOR, TC, and MNZ in 3-CoBM-vis-PMS system (NOR/TC/MNZ = 20 mg/L, PMS = 25 mg, 3-CoBM = 30 mg)

in Fig. 7e. The extremely significant effect of the presence of $HCO_3^-$ on the degradation decreased from 100 to 14.19%. The reason for this investigation is the potent scavenging influence of $HCO_3^-$ on the reactivity species (•OH, $SO_4^{-}$•, and $h^+$, as shown in Eqs. (4)–(6). In contrast, $NO_3^-$, $SO_4^{2-}$, and $Cl^-$ have different degrees of inhibition on the degradation of NOR, and their degradation efficiencies decrease from 100 to 60.72%, 84.72%, and 87.56%, respectively. The reasons for the decrease in NOR degradation efficiency after $NO_3^-$ addition can be attributed to the following two aspects: one way that $NO_3^-$ could slow down degradation by absorbing part of the light during photocatalysis (Kohantorabi et al. 2021); $NO_3^-$ could also suppress degradation by reacting with the active species (•OH, $SO_4^{-}$•), as shown in Eqs. (7) and (8). As shown in Eqs. (9) and (10), $SO_4^{2-}$ influences the rate of degradation by scavenging the generated •OH and $h^+$. Moreover, degradation was inhibited by $Cl^-$ reaction with •OH and $SO_4^{-}$• to produce active substances with lower oxidation numbers, shown in Eqs. (11) and (12). In addition to the reaction of each of the aforementioned ions with the active group resulting in a reduced reaction rate, $NO_3^-$, $Cl^-$, and $SO_4^{2-}$ could compete with the contaminant for the active site on the surface of the contact catalyst to inhibit degradation (Wen et al. 2018b). The reactions that have discussed are listed below:

$$HCO_3^- + \bullet OH \rightarrow H_2O + CO_3^-\bullet \quad (4)$$

$$HCO_3^- + SO_4^-\bullet \rightarrow HCO_3\bullet + SO_4^{2-} \quad (5)$$

$$HCO_3^- + h^+ \rightarrow H_2O + CO_3^-\bullet \quad (6)$$

$$NO_3^- + \bullet OH \rightarrow NO_3\bullet + OH^- \quad (7)$$

$$NO_3^- + SO_4^-\bullet \rightarrow NO_3\bullet + SO_4^{2-} \quad (8)$$

$$SO_4^{2-} + \bullet OH \rightarrow SO_4^-\bullet + OH^- \quad (9)$$

$$SO_4^{2-} + h^+ \rightarrow SO_4^-\bullet \quad (10)$$

$$Cl^- + SO_4^-\bullet \rightarrow SO_4^{2-} + Cl\bullet \quad (11)$$

$$Cl^- + \bullet OH \rightarrow ClOH^-\bullet \quad (12)$$

In order to determine whether the system can effectively degrade different types of antibiotics, the 3-CoBM-vis-PMS were also applied to degrade NOR, TC, and MNZ in the same environment. As displayed in Fig. 7f, the 3-CoBM-vis-PMS system has good degradation efficiency for NOR, TC, and MNZ within 40 min of photocatalysis. The 100% degradation of TC and NOR could be achieved within 40 min, and the degradation efficiency of MNZ could reach 84.95% within 40 min.

## Degradation mechanism

To explore what active groups during in the 3-CoBM-vis-PMS system, TBA was chosen as the capture agent for •OH, MeOH as the capture agent for •OH and $SO_4^-$•, and $Na_2C_2O_4$ as the capture agent for $h^+$. Figure 8 exhibits the effect of different active species trappers in 3-CoBM-vis-PMS system on NOF degradation. Among them, the addition of $Na_2C_2O_4$ shows the largest decrease in the degradation efficiency of NOF, from 100 to 41.60%, which proves that $h^+$ is the most critical active group in the 3-CoBM-vis-PMS system. Previous studies have demonstrated that $SO_4^-$• and •OH are generally considered as reactive oxygen species produced during activated PMS (Chen et al., 2019). However, $h^+$ is proved as the main active group in this study, indicating that the role of photogenic holes in the photocatalysis of 3-CoBM cannot be ignored. This further confirms the important role of photocatalysis-assisted PMS activation in the degradation of NOF. Furthermore, the degradation efficiency dropped to 59.52% when adding the MeOH, while TBA addition only decreased slightly to 80.16%. Therefore, it can be inferred that the active substance in 3-CoBM-vis-PMS system contains •OH, $SO_4^-$•, and $h^+$. And the degree of activity of the three active groups from strong to weak is $h^+$, $SO_4^-$•, and •OH, respectively, wherein *A* and *B* have little differential contribution rate ($SO_4^-$•:20.64%, •OH: 19.84%).

At the same time, the free radical trapping results were verified by EPR technique using DMPO and TEMPO as spin trapping agents, and the results are proposed in Fig. 8c, d. In the dark, EPR signals of 1:2:1:2:1:2:1 can be observed only after 1 min of DMPO addition, which are attributed to DMPO-$SO_4^-$• and DMPO-•OH, respectively. It can be observed in Fig. 8c that when the visible light is turned on for 1 min, the intensity of characteristic peaks of DMPO-$SO_4^-$• and DMPO-•OH increase, and with the prolongation of time, the intensity of peaks becomes stronger at 5 min. Figure 8d showed intensity of characteristic peaks of TEMPO-$h^+$ in the 3-CoBM-vis-PMS system (Fig. 8d, 1

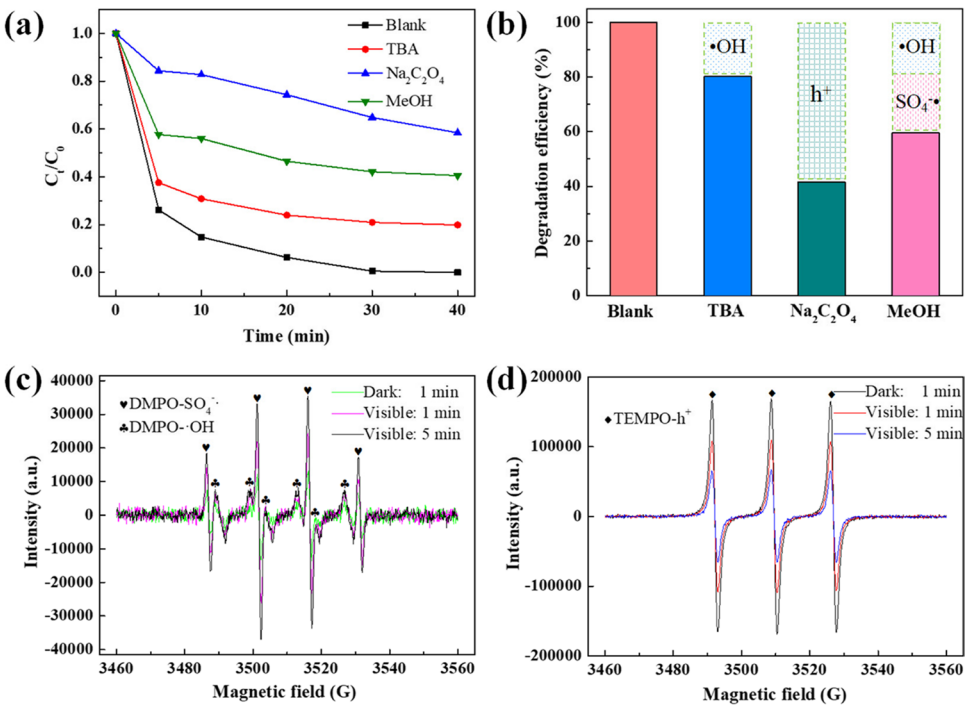


**Fig. 8** **a**, **b** Degradation efficiency of 3-CoBM-vis-PMS system on different active species trappers (NOR = 20 mg/L, PMS = 25 mg, 3-CoBM = 30 mg); **c**, **d** EPR spectra of 3-CoBM-PMS or 3-CoBM-vis-PMS system (3-CoBM = 5 mg, DMPO = 50 mM, TEMPO = 50 mM)

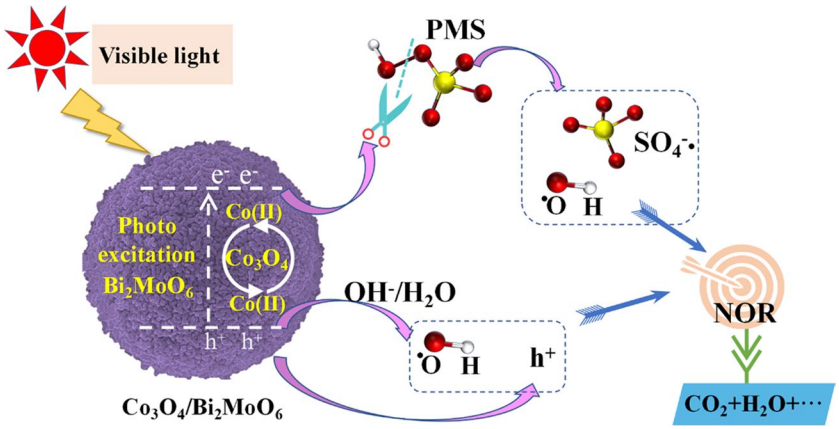


**Scheme 2** Schematic diagram of possible degradation mechanism of $Co_3O_4/Bi_2MoO_6$ driving superior catalytic oxidation for norfloxacin (NOR) removal in a peroxymonosulfate (PMS)/visible light (Vis) system

min/5 min) are weaker than that of the 3-CoBM-PMS system (Fig. 8d, 1 min). The cause for these phenomena is that TEMPO captures $h^+$ generated by 3-CoBM under visible irradiation, resulting in non-paramagnetic TEMPOH, which reduces the intensity of EPR spectrum (Scheme 2).

## Intermediates identification and degradation pathway derivation

In order to explore the possible degradation pathway of NOR, the intermediate products in the process of degradation of NOR in the 3CoBM-vis-PMS system were analyzed by LC-MS. As shown in the supporting information Table S1 and Fig. S1, for NOR, a protonated form of $m/z = 320$ molecular (Wang et al. 2021a) was observed, and a total of 18 possible intermediates (N1-N18) and their molecular structures were identified. Combined with the results of mass spectrometry analysis and related literatures reported by predecessors, four possible degradation pathways are proposed and plotted in Fig. 9. According to the existing literature, the piperazinyl ring in NOR was a reactive group to be attacked by reactive oxygen species (ROS) (Sun et al. 2022b, Zhao et al. 2023), which decomposes the structure of NOR by attacking quinolones and piperazine groups. Generally, the degradation of NOR mainly focuses on the defluorination, decarboxylation, piperazine ring, and quinolone group transformation (Wu et al. 2020).

As can be seen from path I in Fig. 9, after the NOR was continuously attacked by the active oxide, the piperazine ring was opened to form N1 with $m/z = 350$) (Liu et al. 2020). The amino compound N2 ($m/z = 336$) was composed of cleavage and structural rearrangement of the–NH–CH—O group in the hydroxylation product N1 (Chen & Chu 2015). N3 ($m/z = 294$) was formed by further decarbonylation, and the -NH-$CH_2$-$CH_2$-$NH_2$ group of N3 was carbonized to form N4 ($m/z = 279$) after free radical attack. N5 ($m/z = 251$) is formed by N4 decarbonylation. Due to the high electron density on the benzene ring, free radicals attack the benzene ring on N5 and further open the ring to generate N6 ($m/z = 212$) (Guo et al. 2021). It is worth noting that the LC-MS results show that N5 and N6 were abundant, which may prove that path I was the important way for the degradation of NOR in 3CoBM-vis-PMS system. It can be analyzed from path II that NOR obtains N7 ($m/z = 276$) by decarboxylation reaction and then forms N9 ($m/z = 244$) by demethylation and defluorination. The piperazine group on N9 was attacked by free radicals and further oxidized to form N10 ($m/z = 160$) and N11 ($m/z = 146$). In path III, NOR achieves the structural transformation of the intermediate product through the decarboxylation of the carboxyl group on the naphthyridine ring, and the attack of the free radical on the piperazine ring (Ding et al. 2017, Sayed et al. 2016). Therefore, the rapid degradation reaction path was formed by obtaining three structures of the products N12, N13, and N14 with $m/z$ of 296, 270, and 227, respectively. In addition, path IV was a classical defluorination process, including defluorination reaction, decarboxylation reaction, and hydroxylation reaction. N15 ($m/z = 302$) may be due to the defluorination reaction. Then, N15 was further transferred to N16 ($m/z = 318$) by hydroxylation reaction. N17 ($m/z = 257$) was obtained by decarboxylation and hydroxylation of N16. Finally, the piperazine ring of N17 was opened under the attack of active oxides to form N18 ($m/z = 151$). Based on the degradation mechanism of NOR, the four degradation reaction pathways occur simultaneously. In addition, there were many intermediates in other pathways. Overall, these intermediates will eventually be degraded into $CO_2$, $H_2O$, and other low molecular weight organics.

## Conclusion

We have designed successful fabrication of visible light-driven $Co_3O_4/Bi_2MoO_6$ hybrid-architectures nanocomposites by solvothermal synthesis and calcination method and then activating PMS to form a photocatalysis-Fenton

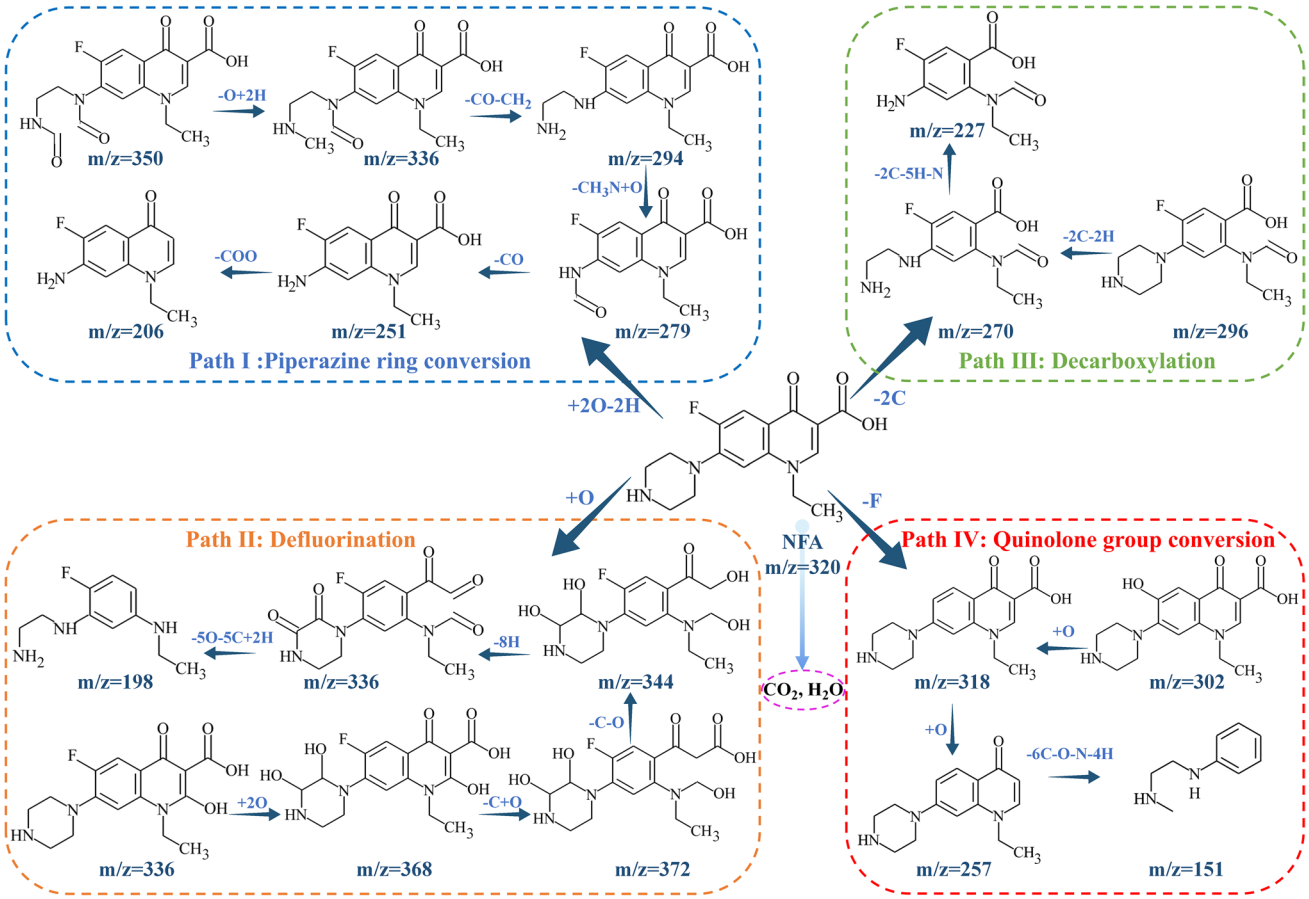


**Fig. 9** Proposed pathways for NOR degradation in 3-CoBM-vis-PMS system

synergy system. The composite catalytic material of $Co_3O_4$ derived from ZIF-67 and the 3-CoBM obtained by calcination at 300 °C had the highest catalytic activity. The XRD and morphological results show that ZIF-67 has been completely converted to $Co_3O_4$, and a too high temperature will destroy the structure of ZIF-67 itself. The good crystallinity, photoresponsive properties, and unique microspherical structure of 3-CoBM show excellent catalytic performance for a variety of antibiotics. Through activating PMS under visible-light irradiation, 84.95% MNZ can be degraded; NOR and TC can be fully degraded within 40 min using 3-CoBM. According to the results of radicals quenching tests and ESR analysis, the efficient degradation of 3-CoBM can be attributed to the combined action of various free radicals. LC-MS analysis results show that the principal oxidation pathways of NOR are defluorination, decarboxylation, and piperazinyl ring transformation, and NOR is finally oxidized to fluoride and nitrate. The $h^+$, •OH, and $SO_4^{-}$• radicals are dominant functional radicals in 3-CoBM-vis-PMS system, and the most important reactive free radical is $h^+$. This work not only provided an approach to synthesize hybrid-architectures nanocomposites but also suggests that the 3-CoBM-vis-PMS system may be a viable choice for environmental remediation to remove resistant organic compounds from wastewater. Considering that, in practical applications, antibiotics may be faced in extreme water bodies, the adaptation of the materials to extreme acidic and alkaline environments should be improved in order to broaden the scope of application of the $Co_3O_4/Bi_2MoO_6$ series materials.

**Supplementary Information** The online version contains supplementary material available at https://doi.org/10.1007/s11356-023-27674-y.

**Author contributions** Qing Sun: conceptualization, data curation, revising, and funding acquisition. Xiaofang Hu: experiment and writing original draft. Yingjie Zhao: experiment and data curation. Jian Zhang: resources. Jiawei Sheng: project administration, review and editing, and funding acquisition. All authors read and approved the final manuscript.

**Funding** This work was financially supported by the Engineering Research Center of Non-metallic Minerals of Zhejiang Province (ZD2023K04), Joint Fund of Zhejiang Provincial Natural Science Foundation-Qing Shan Lake Science and Technology City (LQY19E020002), Technology Program of ZJUT (KYY-HX-20200382; KYY-HX-20220650), and National Natural Science Foundation of China (51604242).

**Data availability** The datasets generated during and/or analyzed during the current study are available from the corresponding author on reasonable request.

## Declarations

**Ethics approval** This article does not contain any studies with human participants or animals performed by any of the authors.

**Consent to participate** All authors have given their consent to participate in submitting this manuscript to this journal.

**Consent for publication** All authors have given their consent to publish this paper in this journal.

**Competing interests** The authors declare no competing interests.

## References


Alhamd M, Tabatabaie T, Parseh I, Amiri F, Mengelizadeh N (2021) Magnetic $CuNiFe_2O_4$ nanoparticles loaded on multi-walled carbon nanotubes as a novel catalyst for peroxymonosulfate activation and degradation of reactive black 5. Environ Sci Pollut Res 28:57099–57114

Alizadeh Z, Rezaee A (2022) Tetracycline removal using microbial cellulose@nano-$Fe_3O_4$ by adsorption and heterogeneous Fenton-like processes. J Mol Liq 366:120199

Alizadeh Z, Jonoush ZA, Rezaee A (2023) Three-dimensional electro-Fenton system supplied with a nanocomposite of microbial cellulose/$Fe_3O_4$ for effective degradation of tetracycline. Chemosphere 317:137890

Aseman-Bashiz E, Rezaee A, Moussavi G (2021) Ciprofloxacin removal from aqueous solutions using modified electrochemical Fenton processes with iron green catalysts. J Mol Liq 324:114694

Biswal BK, Balasubramanian R (2022) Adsorptive removal of sulfonamides, tetracyclines and quinolones from wastewater and water using carbon-based materials: recent developments and future directions. J Clean Prod 349:131421

Cai M, Liu Y, Dong K, Wang C, Li S (2023) A novel S-scheme heterojunction of $Cd_{0.5}Zn_{0.5}S$/BiOCl with oxygen defects for antibiotic norfloxacin photodegradation: performance, mechanism, and intermediates toxicity evaluation. J Colloid Interface Sci 629:276–286

Chen M, Chu W (2015) Photocatalytic degradation and decomposition mechanism of fluoroquinolones norfloxacin over bismuth tungstate: experiment and mathematic model. Appl Catal B: Environ 168-169:175–182

Chen X, Zhou J, Zhang T, Ding L (2019) Enhanced degradation of tetracycline hydrochloride using photocatalysis and sulfate radical-based oxidation processes by Co/$BiVO_4$ composites. J Water Process Eng 32:100918

Ding D, Liu C, Ji Y, Yang Q, Chen L, Jiang C, Cai T (2017) Mechanism insight of degradation of norfloxacin by magnetite nanoparticles activated persulfate: identification of radicals and degradation pathway. J Chem Eng 308:330–339

Feng Q, Zhou J, Zhang Y (2019) Coupling $Bi_2MoO_6$ with persulfate for photocatalytic oxidation of tetracycline hydrochloride under visible light. J Mater Sci Mater Electron 30:19108–19118

Gao H, Yang H, Xu J, Zhang S, Li J (2018) Strongly coupled g-$C_3N_4$ nanosheets-$Co_3O_4$ quantum dots as 2D/0D heterostructure composite for peroxymonosulfate activation. Small:e1801353

Gao Z, Yang H, Cao Y, Wu Q, Kang L, Mao J, Wu J (2019) Complete mineralization of a humic acid by $SO_4\cdot-$ generated on $CoMoO_4$/$gC_3N_4$ under visible-light irradiation. Nanotechnology 30:255704

García-Muñoz P, Zussblatt NP, Pliego G, Zazo JA, Fresno F, Chmelka BF, Casas JA (2019) Evaluation of photoassisted treatments for norfloxacin removal in water using mesoporous $Fe_2O_3$-$TiO_2$ materials. J Environ Manage 238:243–250

Ghanbari F, Moradi M (2017) Application of peroxymonosulfate and its activation methods for degradation of environmental organic pollutants: review. J Chem Eng 310:41–62

Ghanbari F, Martínez-Huitle CA (2019) Electrochemical advanced oxidation processes coupled with peroxymonosulfate for the treatment of real washing machine effluent: a comparative study. J Electroanal Chem 847:113182

González-Pleiter M, Gonzalo S, Rodea-Palomares I, Leganés F, Rosal R, Boltes K, Marco E, Fernández-Piñas F (2013) Toxicity of five antibiotics and their mixtures towards photosynthetic aquatic organisms: implications for environmental risk assessment. Water Res 47:2050–2064

Guo J, Shen C-H, Sun J, Xu X-J, Li X-Y, Fei Z-H, Liu Z-T, Wen X-J (2021) Highly efficient activation of peroxymonosulfate by $Co_3O_4$/$Bi_2MoO_6$ p-n heterostructure composites for the degradation of norfloxacin under visible light irradiation. Sep Purif Technol 259:118109

Hassani A, Eghbali P, Kakavandi B, Lin K-YA, Ghanbari F (2020) Acetaminophen removal from aqueous solutions through peroxymonosulfate activation by $CoFe_2O_4$/mpg-$C_3N_4$ nanocomposite: insight into the performance and degradation kinetics. Environ Technol Innov 20:101127

Huang Y, Nengzi L-c, Zhang X, Gou J, Gao Y, Zhu G, Cheng Q, Cheng X (2020) Catalytic degradation of ciprofloxacin by magnetic CuS/$Fe_2O_3$/$Mn_2O_3$ nanocomposite activated peroxymonosulfate: influence factors, degradation pathways and reaction mechanism. Chem Eng J (Lausanne, Switzerland: 1996) 388:124274

Jadhav HS, Bandal HA, Ramakrishna S, Kim H (2022) Critical review, recent updates on zeolitic imidazolate framework-67 (ZIF-67) and its derivatives for electrochemical water splitting. Adv Mater 34:2107072

Kohantorabi M, Moussavi G, Mohammadi S, Oulego P, Giannakis S (2021) Photocatalytic activation of peroxymonosulfate (PMS) by novel mesoporous Ag/ZnO@$NiFe_2O_4$ nanorods, inducing radical-mediated acetaminophen degradation under UVA irradiation. Chemosphere 277:130271

Li K, Zhang Y, Wang P, Long X, Zheng L, Liu G, He X, Qiu J (2022) Core-Shell ZIF-67@ZIF-8-derived multi-dimensional cobalt-nitrogen doped hierarchical carbon nanomaterial for efficient oxygen reduction reaction. J Alloys Compd 903:163701

Li M-C, Ghanbari F, Chang F-C, Hu C, Lin K-YA, Du Y (2020) Enhanced degradation of 5-sulfosalicylic acid using peroxymonosulfate activated by ordered porous silica-confined $Co_3O_4$ prepared via a solvent-free confined space strategy. Sep Purif Technol 249:116972

Liu B, Song W, Wu H, Liu Z, Teng Y, Sun Y, Xu Y, Zheng H (2020) Degradation of norfloxacin with peroxymonosulfate activated by nanoconfinement $Co_3O_4$@CNT nanocomposite. Chem Eng J 398:125498

Lu Y, Zhan W, He Y, Wang Y, Kong X, Kuang Q, Xie Z, Zheng L (2014) MOF-templated synthesis of porous $Co_3O_4$ concave nanocubes with high specific surface area and their gas sensing properties. ACS Appl Mater Interfaces 6:4186–4195

Özcan A, Atılır Özcan A, Demirci Y (2016) Evaluation of mineralization kinetics and pathway of norfloxacin removal from water by electro-Fenton treatment. Chem Eng J 304:518–526

Pan S, Guo X, Li R, Hu H, Yuan J, Liu B, Hei S, Zhang Y (2022) Activation of peroxymonosulfate via a novel UV/hydrated Fe(III) oxide coupling strategy for norfloxacin removal: performance and mechanism. Sep Purif Technol 300:121909

Peng Y, Tang H, Yao B, Gao X, Yang X, Zhou Y (2021) Activation of peroxymonosulfate (PMS) by spinel ferrite and their composites in degradation of organic pollutants: a review. Chem Eng J 414:128800

Sayed M, Khan JA, Shah LA, Shah NS, Khan HM, Rehman F, Khan AR, Khan AM (2016) Degradation of quinolone antibiotic, norfloxacin, in aqueous solution using gamma-ray irradiation. Environ Sci Pollut Res Int 23:13155–13168

Sayed M, Khan JA, Shah LA, Shah NS, Shah F, Khan HM, Zhang P, Arandiyan H (2017) Solar light responsive poly(vinyl alcohol)-assisted hydrothermal synthesis of immobilized $TiO_2$/Ti film with the addition of peroxymonosulfate for photocatalytic degradation of ciprofloxacin in aqueous media: a mechanistic approach. J Phys Chem C 122:406–421

Senasu T, Nijpanich S, Juabrum S, Chanlek N, Nanan S (2021) CdS/BiOBr heterojunction photocatalyst with high performance for solar-light-driven degradation of ciprofloxacin and norfloxacin antibiotics. Appl Surf Sci 567:150850

Shen Z, Zhou H, Pan Z, Guo Y, Yuan Y, Yao G, Lai B (2020a) Degradation of atrazine by $Bi_2MoO_6$ activated peroxymonosulfate under visible light irradiation. J Hazard Mater 400:123187

Shen Z, Zhou H, Pan Z, Guo Y, Yuan Y, Yao G, Lai B (2020b) Degradation of atrazine by $Bi_2MoO_6$ activated peroxymonosulfate under visible light irradiation. J Hazard Mater 400:123187

Sun Q, Ke M, Zhao Y, Wang B, Zhang J, Sheng J (2021) Embellishing {001} surface of $Bi_2MoO_6$ nanobelts with enhanced photocatalytic performance and mechanisms exploration. Appl Surf Sci 563:150104

Sun Q, Zhao J, Hu Z, Zhang J, Yan J, Sheng J (2022a) Novel fabrication of rod-like $CoAl_2O_4$/halloysite hybrid pigment derived from Co-MOF/nano-clay and mechanism exploration. Dyes Pigm 201:110216

Sun Q, Zhao Y, Zhang J, Sheng J (2022b) Efficient degradation of antibiotics over Co(II)-doped $Bi_2MoO_6$ nanohybrid via the synergy of peroxymonosulfate activation and photocatalytic reaction under visible irradiation. Chemosphere 302:134807

Sun Q, Zhao Y, Zhang J, Sheng J (2022c) Efficient degradation of antibiotics over Co(II)-doped $Bi_2MoO_6$ nanohybrid via the synergy of peroxymonosulfate activation and photocatalytic reaction under visible irradiation. Chemosphere 302:134807

Tang C, Liu E, Wan J, Hu X, Fan J (2016) $Co_3O_4$ nanoparticles decorated $Ag_3PO_4$ tetrapods as an efficient visible-light-driven heterojunction photocatalyst. Appl Catal B: Environ 181:707–715

Wammer KH, Korte AR, Lundeen RA, Sundberg JE, McNeill K, Arnold WA (2013) Direct photochemistry of three fluoroquinolone antibacterials: norfloxacin, ofloxacin, and enrofloxacin. Water Res 47:439–448

Wang C, Kim J, Malgras V, Na J, Lin J, You J, Zhang M, Li J, Yamauchi Y (2019a) Metal–organic frameworks and their derived materials: emerging catalysts for a sulfate radicals-based advanced oxidation process in water purification. Small 15:1900744

Wang C, Yu G, Chen H, Wang J (2021a) Degradation of norfloxacin by hydroxylamine enhanced fenton system: kinetics, mechanism and degradation pathway. Chemosphere 270:129408

Wang L-L, Battini N, Bheemanaboina RRY, Zhang S-L, Zhou C-H (2019b) Design and synthesis of aminothiazolyl norfloxacin analogues as potential antimicrobial agents and their biological evaluation. Eur J Med Chem 167:105–123

Wang L, Luo D, Yang J, Wang C (2022) Metal-organic frameworks-derived catalysts for contaminant degradation in persulfate-based advanced oxidation processes. J Clean Prod 375:134118

Wang M, Yu H, Wang P, Chi Z, Zhang Z, Dong B, Dong H, Yu K, Yu H (2021b) Promoted photocatalytic degradation and detoxication performance for norfloxacin on Z-scheme phosphate-doped $BiVO_4$/graphene quantum dots/P-doped g-$C_3N_4$. Sep Purif Technol 274:118692

Wang R, Ma X, Liu T, Li Y, Song L, Tjong SC, Cao L, Wang W, Yu Q, Wang Z (2020a) Degradation aspects of endocrine disrupting chemicals: a review on photocatalytic processes and photocatalysts. Appl. Catal A: General:597

Wang Y, Wu Y, Yu Y, Pan T, Li D, Lambropoulou D, Yang X (2020b) Natural polyphenols enhanced the Cu(II)/peroxymonosulfate (PMS) oxidation: the contribution of Cu(III) and HO•. Water Res 186:116326

Wen X-J, Niu C-G, Guo H, Zhang L, Liang C, Zeng G-M (2018a) Photocatalytic degradation of levofloxacin by ternary $Ag_2CO_3$/$CeO_2$/AgBr photocatalyst under visible-light irradiation: degradation pathways, mineralization ability, and an accelerated interfacial charge transfer process study. J Catal 358:211–223

Wen X-J, Niu C-G, Zhang L, Liang C, Guo H, Zeng G-M (2018b) Photocatalytic degradation of ciprofloxacin by a novel Z-scheme $CeO_2$–Ag/AgBr photocatalyst: influencing factors, possible degradation pathways, and mechanism insight. J Catal 358:141–154

Wu D, Zhang X, Liu S, Ren Z, Xing Y, Jin X, Ni G (2022) Fabrication of a Z-scheme $CeO_2$/$Bi_2O_4$ heterojunction photocatalyst with superior visible-light responsive photocatalytic performance. J Alloys Compd 909:164671

Wu X, Kim J-H (2022) Outlook on single atom catalysts for persulfate-based advanced oxidation. ACS ES&T Eng 2:1776–1796

Wu Y, Li Y, He J, Fang X, Hong P, Nie M, Yang W, Xie C, Wu Z, Zhang K, Kong L, Liu J (2020) Nano-hybrids of needle-like $MnO_2$ on graphene oxide coupled with peroxymonosulfate for enhanced degradation of norfloxacin: a comparative study and probable degradation pathway. J Colloid Interface Sci 562:1–11

Yin N, Chen H, Yuan X, Zhang Y, Zhang M, Guo J, Zhang Y, Qiao L, Liu M, Song K (2022) Highly efficient photocatalytic degradation of norfloxacin via $Bi_2Sn_2O_7$/PDIH Z-scheme heterojunction: influence and mechanism. J Hazard Mater 436:129317

Zhang B, Zhang M, Zhang L, Bingham PA, Tanaka M, Li W, Kubuki S (2021) BiOBr/$MoS_2$ catalyst as heterogenous peroxymonosulfate activator toward organic pollutant removal: energy band alignment and mechanism insight. J Colloid Interface Sci 594:635–649

Zhao Y, Sun Q, Zhang J, Sheng J (2023) Construction of Fe/N/C nanoclusters anchored on porous diatomite for efficient removal of norfloxacin via the adsorption-PMS activation. Sep Purif Technol 310:123127

Zhao Z, Zhang W, Sun Y, Yu J, Zhang Y, Wang H, Dong F, Wu Z (2016) Bi cocatalyst/$Bi_2MoO_6$ microspheres nanohybrid with SPR-promoted visible-light photocatalysis. J Phys Chem C 120:11889–11898

Zhou K, Mousavi B, Luo Z, Phatanasri S, Chaemchuen S, Verpoort F (2017) Characterization and properties of Zn/Co zeolitic imidazolate frameworks vs. ZIF-8 and ZIF-67. J Mater Chem 5:952–957

Zhu L, Shen D, Zhang H, Luo KH, Li C (2023) Fabrication of Z-scheme $Bi_7O_9I_3$/g-$C_3N_4$ heterojunction modified by carbon quantum dots for synchronous photocatalytic removal of Cr (VI) and organic pollutants. J Hazard Mater 446:130663